

Klein bound states in single-layer graphene

Y. Avishai^{1,2,3} and Y. B. Band^{1,4}

¹*Department of Physics and The Ilse Katz Center for Nano-Science, Ben-Gurion University of the Negev, Beer-Sheva, Israel*

²*New-York Shanghai University, 1555 Century Avenue, Shanghai, China*

³*Yukawa Institute for Theoretical Physics, Kyoto, Japan*

⁴*Department of Chemistry, Ben-Gurion University of the Negev, Beer-Sheva, Israel*

 (Received 10 April 2020; revised 9 August 2020; accepted 16 August 2020; published 31 August 2020)

The Klein paradox, introduced in the study of chiral tunneling in single-layer graphene, is shown to also manifest in graphene bound states with a 1D square-well potential. Such bound states occur both below and above the potential well. We derive bound-state wave functions, in the absence and in the presence of an external transverse magnetic field, and calculate the corresponding electronic currents and dipole transition rates, which can be experimentally probed. The role of parity and time-reversal symmetries is discussed. Our results are also relevant for the physics of bound states of light in periodic optical waveguide structures.

DOI: [10.1103/PhysRevB.102.085435](https://doi.org/10.1103/PhysRevB.102.085435)

I. INTRODUCTION

Chiral tunneling of electrons through a 1D potential barrier in single layer graphene in which the Klein paradox [1] is exposed was first considered in a seminal paper by Katsnelson, Novoselov, and Geim [2]. It was studied experimentally [3,4] and theoretically [5,6], and stimulated much research on the topic of potential scattering of electrons in graphene [6–10]. A closely related and physically motivated problem concerns the formation of electron bound states in graphene [8,9,11–14] (the notion of bound states refers here to electrons bound along x and free to move along y).

Here we consider the occurrence of confined electrons in single layer graphene subject to a symmetric 1D square well potential, $U(x) = U(-x)$, of height U_0 , and elucidate several novel aspects of such bound states that are amenable to experimental verification. We also explore the transmission coefficient at energy E , $T(\varepsilon)$, for Klein scattering off a single barrier in the two cases $0 < E < U_0$ and $E > U_0 > 0$. First, we consider bound states in the absence of an external magnetic field and significantly expand upon earlier results reported in Refs. [8,9] (see our list of main results below). Second, we consider the occurrence of bound states in the presence of a uniform perpendicular magnetic field (this topic has not been discussed earlier).

Our main results are: (1) In the absence of a magnetic field, analytic expressions for bound-state eigenfunctions and eigenvalues are obtained, and electric dipole transition strengths are calculated to determine the absorption spectrum between bound states. Parity and time reversal symmetries are employed to find the relation between the two (pseudo)spinor components of the wave function. Klein tunneling and occurrence of bound states are analyzed in the entire energy range. In particular, we show that Klein bound states occur in both cases $E > U_0$ (bound states above the barrier) and $E < U_0$. (2) In the presence of an external magnetic field, analytic expressions for the bound state wave functions for a discrete

sequence of potential strengths, and numerical solutions for any potential strength are derived. These solutions are then used to determine the measurable areal densities and currents. Based on ideas presented in Refs. [15,16], our formalism also applies to the occurrence of bound states of light in periodic optical waveguide structures.

The outline of the paper is as follows. Section II considers the bound state is a symmetric 1D square well $U(x) = U(-x)$. Section III presents the energy eigenvalues, wave functions, symmetries, and currents in the Klein regime, and Sec. IV presents calculation of the electromagnetic transitions between the bound states. In Sec. V we trace the behavior of Klein transmission for scattering off a rectangular barrier and Klein bound states in a square well in the entire energy range $E > 0$. The analysis of bound states in a combination of perpendicular magnetic field and square well is developed in Sec. VI, and finally, Sec. VII presents a short summary and conclusion. Several technical issues are relegated to the Appendix.

II. BOUND STATES IN A SYMMETRIC 1D SQUARE WELL

Recall that graphene can be treated as two interpenetrating triangular lattices often labeled by A and B [17]. In the presence of an external potential $U(x, y)$, the dynamics of the low-energy quasiparticles of the system near the Dirac points (say \mathbf{K}') is governed by the 2D Dirac Hamiltonian for massless particles: $H = \gamma \boldsymbol{\sigma} \cdot \mathbf{p} + U(x, y)$ [2]. Here $\boldsymbol{\sigma}$ is the pseudospin Pauli matrix vector, $\mathbf{p} = (p_x, p_y)$ is the 2D momentum operator, and $\gamma = \hbar v_F$ in which $v_F \approx 10^8$ cm/sec is the Fermi velocity. We search for bound states (energies and wave functions) of a massless particle in single-layer graphene using the 2D Dirac equation with 1D square-well symmetric potential $U(x) = U_0 \Theta(|x| - L)$.

To simplify manipulations, it is useful to define dimensionless variables. The square-well half-width $L = 100$ nm can serve as a length unit. Henceforth dimensionless coordinates

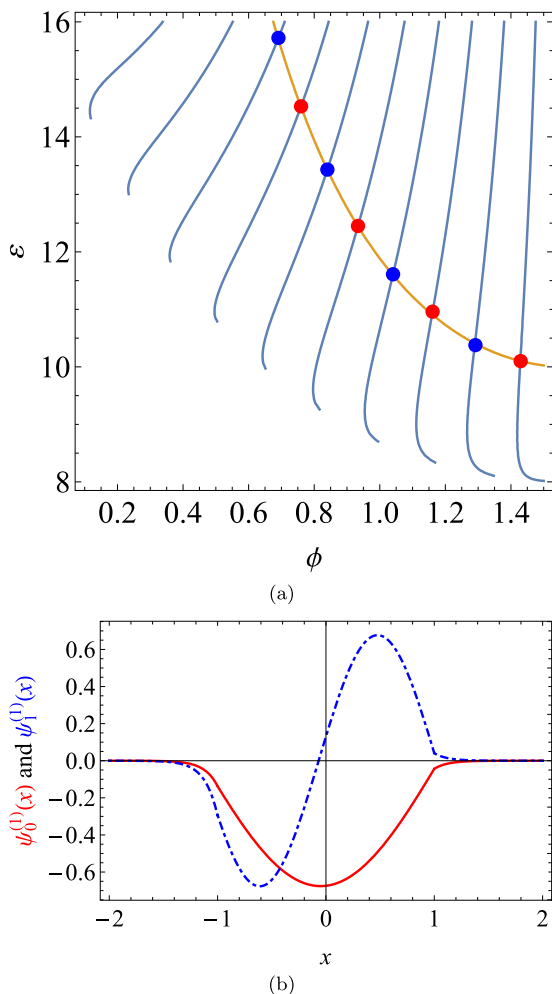


FIG. 1. (a) Nodes of $\det[A(\varepsilon, \phi)]$, Eq. (5), in the (ϕ, ε) plane (blue curves), and the curve $k_y = \varepsilon \sin \phi = 10$ (orange curve). The pairs (ε_n, ϕ_n) specified by blue and red dots are the bound state energies for this fixed k_y . The spectrum is discrete for $k_y > u_0/2$. (b) Upper components of $\psi_0(x)$ (red solid curve) and $\psi_1(x)$ (blue dot-dashed curve) versus x . The lower components are related to the upper ones via Eq. (8). Note that the wave functions do not have a definite symmetry around $x = 0$ (see discussion on the role of parity below).

and wave numbers are defined as $x \rightarrow x/L$, $y \rightarrow y/L$, $k \rightarrow kL$. The energy $\varepsilon_0 \equiv \gamma/L = 6.538$ meV serves as an energy unit, so that the dimensionless energy is $\varepsilon = E/\varepsilon_0$ (where E is the energy in meV), and the dimensionless potential is $u(x) = U(x)/\varepsilon_0$. For definiteness we take $U_0/\varepsilon_0 \equiv u_0 = 16$, which implies $U_0 = 104.613$ meV (the value of U_0 is close to that used in Fig. 2 of Ref. [2]).

Klein physics [1] occurs for $u_0 > \varepsilon > 0$ where inside the well ($|x| < 1$) the Fermi energy lies in the conduction band while outside the well ($|x| > 1$) the Fermi energy lies in the valence band [1,6]. Near the \mathbf{K}' Dirac point, the time-independent 2D Dirac equation (in dimensionless variables) is

$$\mathcal{H}\Psi \equiv [-i(\sigma_x \partial_x + \sigma_y \partial_y) + u(x)]\Psi(x, y) = \varepsilon\Psi(x, y). \quad (1)$$

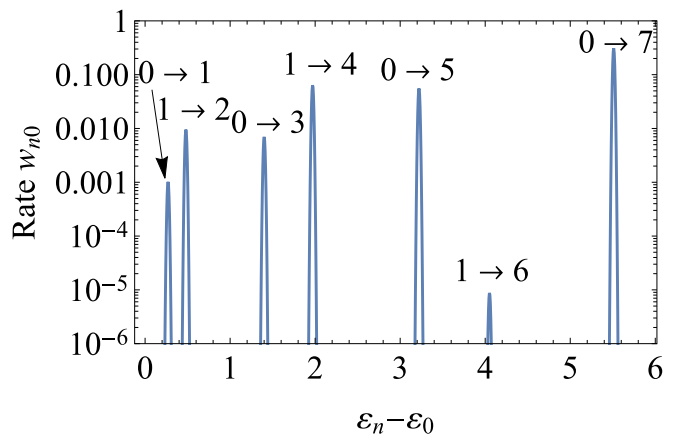


FIG. 2. Absorption spectrum of the transitions $0 \rightarrow 1$, $0 \rightarrow 3$, $0 \rightarrow 5$, $0 \rightarrow 7$, $1 \rightarrow 2$, $1 \rightarrow 4$, $1 \rightarrow 6$. The absorption rate w_{mn} (in dimensionless units) from level n to m is plotted versus the resonant absorption photon energy $\hbar\omega_{nm} = \varepsilon_n - \varepsilon_m$ (in dimensionless units).

Under parity transformation $(x, y) \rightarrow (-x, y)$, the potential is symmetric, $u(x) = u(-x)$, but the total Hamiltonian is not, $\mathcal{H}(-x, y) \neq \mathcal{H}(x, y)$. The general solution of the wave function in the three different regions is $\Psi(x, y) = e^{ik_y y} \psi(x)$,

$$\psi(x) = \begin{cases} a \begin{pmatrix} 1 \\ e^{i\phi} \end{pmatrix} e^{ik_x x} + b \begin{pmatrix} 1 \\ -e^{-i\phi} \end{pmatrix} e^{-ik_x x} & (|x| < 1), \\ \alpha \begin{pmatrix} 1 \\ -e^{i\theta} \end{pmatrix} e^{iq_x x} + \beta \begin{pmatrix} 1 \\ e^{-i\theta} \end{pmatrix} e^{-iq_x x} & (x > 1), \\ \gamma \begin{pmatrix} 1 \\ -e^{i\theta} \end{pmatrix} e^{iq_x x} + \delta \begin{pmatrix} 1 \\ e^{-i\theta} \end{pmatrix} e^{-iq_x x} & (x < -1), \end{cases} \quad (2)$$

where ϕ is the inclination angle in the x - y plane and θ is the refractive angle [6]. The dimensionless wave number vector inside the well [where $u(x) = 0$] is $\mathbf{k} = \varepsilon(\cos \phi \hat{\mathbf{x}} + \sin \phi \hat{\mathbf{y}}) \equiv k_x \hat{\mathbf{x}} + k_y \hat{\mathbf{y}}$, and $|\mathbf{k}| = \varepsilon = \sqrt{k_x^2 + k_y^2}$. The x component of the momentum outside the well [where $u(x) = u_0 > 0$], q_x , and the refractive angle θ are

$$q_x = \sqrt{(\varepsilon - u_0)^2 - k_y^2},$$

$$\tan \theta = \frac{k_y}{q_x} = \frac{\varepsilon \sin \phi}{\sqrt{(\varepsilon - u_0)^2 - (\varepsilon \sin \phi)^2}}. \quad (3)$$

In the p - n - p junction analyzed here, Klein tunneling occurs for $u_0/(1 + \sin \phi) > \varepsilon > 0$, so that q_x is real, whereas Klein bound states occur for $u_0 > \varepsilon > u_0/(1 + \sin \phi) > 0$, so that q_x is imaginary,

$$q_x = i\kappa_x(\varepsilon, \phi) \equiv i\sqrt{(\varepsilon \sin \phi)^2 - (u_0 - \varepsilon)^2}, \quad (4)$$

and $\kappa_x(\varepsilon, \phi) > 0$.

The bound state wave functions must decay exponentially as $e^{-\kappa_x |x|}$ as $|x| \rightarrow \infty$. In this region $\tan \theta = -ik_y/\kappa_x$ is pure imaginary, and $\tan^2 \theta < -1$. Consequently, $\sin \theta$ is real and $\cos \theta$ is imaginary. To ensure asymptotic decay at large $|x|$ we must set $\beta = \gamma = 0$ in Eq. (2). Continuity of $\psi(x)$ at $x = \pm 1$ yields a homogeneous system of four linear equations for the complex coefficient vector $\mathbf{c} \equiv (a, b, \alpha, \delta)^T$ that is an eigenvector with zero eigenvalue of the matrix $A(\varepsilon)$, $A(\varepsilon)\mathbf{c} = 0$ [$A(\varepsilon)$ is explicitly given in Eq. (A3) in the Appendix]. The determinant of $A(\varepsilon)$ is

given by

$$C \det[A(\varepsilon)] = \kappa_x(\varepsilon, \phi) \cos \phi \cos(2\varepsilon \cos \phi) + [\varepsilon(1 + \sin^2 \phi) - u_0] \sin(2\varepsilon \cos \phi), \quad (5)$$

where C is a nonvanishing multiplicative constant and the expression on the RHS is real [see Eq. (A5) in the Appendix]. Bound states occur at energies ε_n for which $\det[A(\varepsilon_n)] = 0$. For reasons that will be explained below, we focus on bound states at different energies $\{\varepsilon_n\}$ but for *the same* $k_y = \varepsilon_n \sin \phi_n$. With our parameters, $u_0 = \frac{LU_0}{\hbar v_F} \approx 16.0$, and the pattern of bound state energies in the (ϕ, ε) plane is as shown in Fig. 1(a). Also shown in the figure is the curve $k_y = \varepsilon \sin \phi = 10$ ($= 0.1 \text{ nm}^{-1}$). The intersection points indicate bound-state energies $\{\varepsilon_n\}$ with the same value of $k_y = \varepsilon_n \sin \phi_n$. Note that for this value of k_y , there are no states in the continuum below $u_0 = 16$.

III. WAVE FUNCTIONS, SYMMETRIES, CURRENTS

Once a bound-state energy ε_n is determined through a numerical solution of the transcendental equation $\text{Det}A(\varepsilon) = 0$, evaluation of the corresponding spinor wave functions $\psi_n(x)$ is obtained analytically and exposes a beautiful symmetry between its two components. This symmetry is exploited for the discussion of parity and time-reversal symmetries which reflects on the pattern of currents.

A. Wave functions

Here we compute the wave functions for (ε_n, ϕ_n) , $n = 0, 1, \dots, 7$, see Fig. 1(a). The pairs (ε_n, ϕ_n) are inserted into the matrix A and the spinor bound-state wave functions $\psi_n(x) = \begin{pmatrix} \psi_n^{(1)} \\ \psi_n^{(2)} \end{pmatrix}$ are determined in terms of the four coefficients $\mathbf{c}_n \equiv (a_n, b_n, \alpha_n, \delta_n)$, i.e., the solution of the eigenvalue equation $A(\varepsilon_n, \phi_n)\mathbf{c}_n^T = 0$. Due to parity symmetry (see below), it is possible to choose an overall phase such that the components of the spinors are subject to the following constraints:

$$\begin{aligned} \text{Im}[\psi_n^{(1)}(x)] &= \text{Re}[\psi_n^{(2)}(x)] = 0, \\ \text{Im}[\psi_n^{(2)}(x)] &= (-1)^n \text{Re}[\psi_n^{(1)}(-x)]. \end{aligned} \quad (6)$$

Analytic expressions for the ground and excited state wave functions are derived by choosing

$$a = b^* = \mathcal{A}_n e^{i\eta_n}, \quad \eta_n = (2n+1)\frac{\pi}{4} - \frac{1}{2}\phi, \quad (7)$$

where \mathcal{A}_n are real normalization constants and the phase η_n is chosen to satisfy the symmetries in Eq. (6). Combining Eqs. (2) and (7), the bound-state wave functions, $\Psi_n(x, y) = e^{ik_y y} \psi_n(x)$ for $|x| < 1$ are

$$\begin{aligned} \psi_n(x) &= \mathcal{A}_n \begin{pmatrix} \psi_n^{(1)}(x) \\ (-1)^n i \psi_n^{(1)}(-x) \end{pmatrix} \\ &= \mathcal{A}_n \begin{pmatrix} \cos[\gamma_n^-(x)] + \sin[\gamma_n^-(x)] \\ (-1)^n i \{\cos[\gamma_n^+(x)] + \sin[\gamma_n^+(x)]\} \end{pmatrix}, \end{aligned} \quad (8)$$

where $\gamma_n^\pm(x) = \frac{1}{2}(\phi_n \pm 2k_{nx}x)$ and $k_{nx} = \varepsilon_n \cos \phi_n$. The decaying parts of the wave functions for $|x| > 1$ are determined by the coefficients β , δ , and the symmetry specified in Eq. (6) is fulfilled *for all* x . The two upper components of the spinor wave functions $\psi_{n=0,1}(x)$ are shown in Fig. 1(b).

The symmetry specified in Eq. (6) also implies that $\psi_0^\dagger(x)\psi_1(x)$ is an odd function of x . Hence, $\langle \psi_0 | \psi_1 \rangle = 0$, i.e., the two states are orthogonal, as are any two different eigenfunctions.

B. Discrete symmetries

1. Parity

The importance of parity in the physics of graphene is discussed in Ref. [18], where it is shown that parity operator in $(1+2)$ dimensions plays an interesting role and can be used for defining conserved chiral currents (see also Ref. [19]). Here we concentrate on bound states, wherein the current along x should vanish and consider the role of the parity transformation under which the Hamiltonian is *not* invariant. For a symmetric potential, $u(x) = u(-x)$, we consider the static (time-independent) case with Hamiltonian $\mathcal{H}(x, y)$ introduced in Eq. (1). The parity transformation in $2+1$ dimensions is taken to mean the transformation $(x, y) \rightarrow (-x, y)$. For massless Dirac fermions this transformation is realized by the operator σ_y . Explicitly,

$$\mathcal{H}^P(x, y) = i\sigma_x \partial_x - i\sigma_y \partial_y + u(x), \quad (9)$$

and $\mathcal{H}^P(x, y) \equiv \sigma_y \mathcal{H}(x, y) \sigma_y = \mathcal{H}(-x, y) \neq \mathcal{H}(x, y)$. Thus, near a given Dirac point, say \mathbf{K}' , \mathcal{H} is not parity invariant [even though $u(x) = u(-x)$] [20]. However, for a symmetric potential the wave functions $\psi_n(x)$ in Eq. (8) obeys the symmetry relations,

$$\sigma_y \psi_0(x) = \psi_0(-x), \quad \sigma_y \psi_1(x) = -\psi_1(-x). \quad (10)$$

Equation (10) is a concrete realization of Eq. (14) in Ref. [18]. Hence, we define $\psi_n(x)$ as being $\begin{pmatrix} \text{even} \\ \text{odd} \end{pmatrix}$ under parity if and only if $\sigma_y \psi(x) = \pm \psi(-x)$. With this assignment, Eq. (10) is consistent with (albeit different than) the nonrelativistic one-dimensional problem, where, in a symmetric potential, the parity of eigenstates is such that $\psi_n(-x) = (-1)^n \psi_n(x)$, $n = 0, 1, 2, \dots$, and the ground state is symmetric. By definition, $\mathcal{H}\psi_n(x) = \varepsilon_n \psi_n(x) \Rightarrow \mathcal{H}^P \psi_n(-x) = \varepsilon_n \psi_n(-x)$. Thus, $\psi_n(x)$ and $\psi_n(-x) \neq \pm \psi_n(x)$ are, respectively, eigenfunctions of \mathcal{H} and $\mathcal{H}^P \neq \mathcal{H}$ with the same eigenvalue ε_n .

2. Time reversal invariance

The time reversal operator is $\mathcal{T} = i\sigma_y K$, where K is the complex conjugation operator. It is easy to check that $[\mathcal{H}, \mathcal{T}] = 0$, so that each state is doubly (Kramers) degenerate. Applying the operator \mathcal{T} on a wave function $\Psi_n(x, y)$, Eq. (8) we obtain [recall that $\psi_n^{(1)}(x)$ is real and $\psi_n^{(2)}(x) = (-1)^n i \psi_n^{(1)}(-x)$ is purely imaginary],

$$\Psi_n^{\mathcal{T}}(x, y) = \mathcal{A}_n e^{-ik_y y} \begin{pmatrix} (-1)^n \psi_n^{(1)}(-x) \\ i \psi_n^{(1)}(x) \end{pmatrix}, \quad (11)$$

which is the Kramers partner of $\Psi_n(x, y)$, i.e., $\mathcal{H}\Psi_n^{\mathcal{T}}(x, y) = \varepsilon_n \Psi_n^{\mathcal{T}}(x, y)$.

C. Currents

Bound states, with wave functions $\psi_n(x) = \begin{pmatrix} \psi_n^{(1)}(x) \\ \pm i \psi_n^{(1)}(-x) \end{pmatrix}$, do not carry current along x : $J_{nx}(x) \equiv \psi_n^\dagger(x) \sigma_x \psi_n(x) = 0$. However, they do carry current along y , $J_{ny}(x) \equiv \psi_n^\dagger(x) \sigma_y \psi_n(x) \neq$

0, ($n = 0, 1$), that is symmetric under $x \leftrightarrow -x$ and it quickly decays for $|x| > 1$. As we discuss below in connection with time reversal invariance, all states are Kramers degenerate, and the two degenerate states forming a Kramers pair carry currents in opposite directions. Since the measured current is the incoherent sum of the contributions from the two degenerate Kramers states, it is virtually unobservable. As we shall see below, in the presence of magnetic field the current is observable.

IV. ELECTROMAGNETIC TRANSITIONS

Consider E_1 transitions induced by x polarized light such that the dipole operator is $\mathcal{O}(x) = eE_x x$, where E_x is the electric field amplitude. The parity of the product $\psi_n^\dagger(x)\psi_m(x)$ is $(-1)^{n+m+1}$. Because k_y is conserved and is the same for $\Psi_n(x, y)$ and $\Psi_m(x, y)$, we have $\langle \Psi_m | \mathcal{O} | \Psi_n \rangle = \frac{1}{2} [1 - (-1)^{n+m}] eE_x \langle x \rangle_{n,m}$. Figure 2 shows the absorption spectrum of the transitions $0 \rightarrow 1$, $1 \rightarrow 2$, $0 \rightarrow 3$, $1 \rightarrow 4$, $0 \rightarrow 5$, $1 \rightarrow 6$, $0 \rightarrow 7$, where the absorption rates (in arbitrary units) w_{nm} from m to n are proportional to $\omega_{nm}^4 |\langle \psi_n | x | \psi_m \rangle|^2$ where $\hbar\omega_{nm} = \varepsilon_n - \varepsilon_m$ [21].

Strictly speaking, electrons can occupy wave functions with arbitrary transverse wave number in the range $u_0 - \varepsilon < k_y < \varepsilon$ and E_1 transitions can occur between energy states with different k_y . However, practically, an experiment can be carried out in a graphene nanoribbon of width L_y such that $k_y = \frac{2\pi p}{L_y}$, ($p = 1, 2, \dots$) is quantized. If L_y is sufficiently small, only the lowest mode, $p = 1$, is occupied, and all transitions occur between states of the same value of k_y . In our example, $k_y = 10$ and $\varepsilon < u_0 = 16$ (in dimensionless units). Hence, the second mode ($p = 2$) has $k_y = 20 > \varepsilon$ which is outside of the allowed range. Let us estimate the pertinent value of L_y . Since $k_y L = 10$ and $L = 100$ nm, we have $k_y = 0.1 \text{ nm}^{-1}$ corresponding to a graphene nanoribbon width of $L_y = 132.6$ nm. Experimental fabrication of graphene nanoribbons of similar width is reported in Ref. [22].

V. BOUND STATES AND TRANSMISSION ABOVE THE BARRIER, $\varepsilon > u_0$

Discrete bound states occur under the condition that $q_x^2 = (\varepsilon - u_0)^2 - k_y^2 = (\varepsilon - u_0)^2 - (\varepsilon \sin \phi)^2 < 0$. Thus, we can trace the occurrence of bound states either for fixed ϕ or fixed k_y . Below we will formulate the conditions for $q_x^2 < 0$ for either sign of $\varepsilon - u_0$ in terms of ϕ and/or k_y .

For fixed inclination angle ϕ , and square-well barrier height u_0 we have so far focused on the formation of bound states below the barrier height ($\varepsilon < u_0$), expected for $\frac{u_0}{1+|\sin \phi|} < \varepsilon < u_0$ (equivalently, for fixed transverse wave number the condition for $q_x^2 < 0$ is $u_0 - k_y < \varepsilon < u_0$). Experimentally, it is possible to tune the Fermi energy through the whole interval $\varepsilon > 0$. In this section we briefly substantiate the formation of bound states at energies above the potential barrier, $\varepsilon > u_0$, and, for the sake of completion, we illustrate the behavior of the transmission coefficient $T(\varepsilon)$ along the entire energy interval $\varepsilon > 0$ (its main properties have already been reported in Ref. [6]).

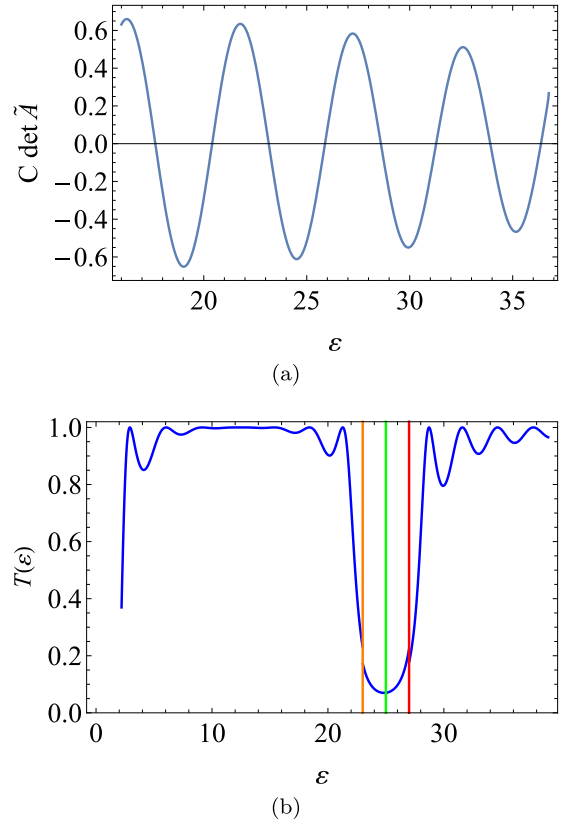


FIG. 3. (a) The determinant of the set of homogeneous equations (up to a multiplicative constant C) versus energy ε whose zeros indicates bound-state energies in a symmetric square well of height $u_0 = 16$ and width $2L = 2$ for $\phi = 0.6$. These bound states occur in the interval for $u_0 < \varepsilon < u_0/(1 - |\sin \phi|)$ (the right part of interval II). (b) For fixed transverse wave number $k_y = 2$, the transmission $T(\varepsilon)$ through a barrier of height $u_0 = 25$, and width $D = 1$ is plotted as a function of energy in the entire energy interval $\varepsilon > k_y$. Referring to the text, the first vertical line on the left (orange) separates regions I and II, and the second vertical line (green) specifies the grazing energy $\varepsilon = u_0$ for which $q_x = ik_y$ and the transmission is minimal. The third vertical line (red) separates regions II and III above which the transmission oscillates as it approaches the unitary limit.

A. Bound states above the barrier

Discrete bound states with energy above the potential barrier height are expected to occur in the interval $\frac{u_0}{1-|\sin \phi|} > \varepsilon > u_0$ wherein $q_x^2 < 0$ (equivalently, for $0 < \varepsilon - u_0 < k_y$). The matrix $\tilde{A}(\varepsilon)$ for the system of matching equations in the region $\varepsilon > u_0$ is different from the matrix $A(\varepsilon)$ in the region $\varepsilon < u_0$ that is defined in Eq. (A3) in the Appendix. Explicitly, $\tilde{A}(\varepsilon)$ is obtained from $A(\varepsilon)$ by reversing the sign of the elements $A(2, 3)$ and $A(4, 4)$. The corresponding determinant $\text{Det}[\tilde{A}(\varepsilon)]$ is given in Eq. (A5) in the Appendix. The bound states in this subregion are then identified as the zeros of $\text{Det}[\tilde{A}(\varepsilon)]$, as shown in Fig. 3(a). These Klein bound states occur above the barrier where both ε and $\varepsilon - u_0$ lie in the conduction band, when $0 < \varepsilon - u_0 < k_y$. Recall that in an analogous Schrödinger problem the condition for occurrence of bound states above the barrier is $0 < \varepsilon - u_0 < k_y^2$. To the best of our knowledge Klein

bound states above the barrier have not been considered so far.

B. The transmission coefficient $T(\varepsilon)$ for the entire positive energy interval

Klein transmission through a rectangular barrier has been studied in Ref. [6]. For fixed transverse wave number k_y , expressions for the transmission coefficient are given at several energies in the interval $0 < k_y < \varepsilon$. For the sake of completeness we specify the relevant energy regions in the plot of $T(\varepsilon)$ versus energy in Fig. 3(b). Guided by Fig. 3(b), it is useful to divide the positive energy axis into three intervals according to the sign of $q_x^2 = (\varepsilon - u_0)^2 - k_y^2$.

(i) Region I: $k_y < \varepsilon < u_0 - k_y$, wherein $q_x^2 > 0$. The wave function is extended, Klein tunneling prevails as studied in Refs. [2,6].

(ii) Region II: $u_0 - k_y < \varepsilon < u_0 + k_y$, wherein $q_x^2 < 0$. The wave function decays under the barrier, and the transmission is exponentially small. In particular, at the grazing energy $\varepsilon = u_0$, $q_x = ik_y$ (maximally imaginary) and the transmission is minimum. For $u_0 < \varepsilon \rightarrow u_0 + k_y$, $q_x^2 \rightarrow 0$, where here \rightarrow means approaching from below, and the transmission increases.

(iii) Region III: $\varepsilon > u_0 + k_y$ we have $q_x^2 > 0$ and the transmission tends to its maximum with oscillations.

We can now summarize the main physical points illustrated in Fig. 3(b): (1) To the left of the first line at $k_y < \varepsilon < u_0 - k_y$ we see that: (1a) Transmission occurs below the barrier and oscillates below its maximum due to Klein chiral tunneling as discussed in Refs. [2,6]. (1b) The wave function in the square well is extended and there are no bound states. (2) Between the first and second vertical lines $u_0 - k_y < \varepsilon < u_0$ we have: (2a) Transmission is very small and decreases with energy to a minimum at the green vertical line erected above the grazing energy $\varepsilon = u_0$, and (2b) there are isolated Klein bound states *under the potential barrier* as analyzed above in the previous sections. (3) Between the second and third lines $u_0 < \varepsilon < u_0 + k_y$ we have: (3a) Transmission occurs above the barrier, but it is small, and increases with energy, and (3b) there are isolated Klein bound states that occur *above the potential barrier* [see Fig. 3(a)]. (4) To the right of the third line $u_0 + k_y < \varepsilon$ we have: (4a) Transmission occurs above the barrier and oscillates with decreasing amplitude and approaches its maximum value and (4b) there are no bound states.

VI. BOUND STATES IN A PERPENDICULAR MAGNETIC FIELD AND SQUARE WELL

Analysis of bound states in the presence of a uniform perpendicular magnetic field and a square well potential enables access to “un-quantized” Landau functions in graphene. First recall the extensively studied case $U(x) = 0$ (see, e.g., Ref. [23]). In the Landau gauge, $A_y = Bx$, translation invariance along y ensues, and the spinor wave function factorizes as $\Psi(x, y) = e^{ik_y y} \psi(x)$. Introducing the magnetic length $\ell = \sqrt{\hbar c / (eB)}$ enables formulation in terms of the dimensionless position, wave number, and binding energy: $x \rightarrow x/\ell$, $k_{x,y} \rightarrow k_{x,y}\ell$ and $\varepsilon = \frac{eE}{\hbar v_F}$. The bare equation with dimensionless

variables and parameters reads:

$$[-i\sigma_x \partial_x + \sigma_y(k_y - x)]\psi(x) = \varepsilon\psi(x). \quad (12)$$

It is simplified after a shift and scaling of the position coordinate, $x \rightarrow \frac{z}{\sqrt{2}} + k_y$, into

$$\mathcal{H}\psi(z) \equiv \left[-i\sigma_x \partial_z - \frac{1}{2}z\sigma_y \right]\psi(z) = \varepsilon\psi(z), \quad (13)$$

whose general solution is (with $\bar{\delta} \equiv 1 - \delta$),

$$\begin{pmatrix} \psi^{(1)}(z) \\ \psi^{(2)}(z) \end{pmatrix} = c_1 \begin{pmatrix} D_{\nu_1}(z) \\ \frac{\varepsilon}{i} D_{\nu_1-1}(z) \end{pmatrix} + c_2 \bar{\delta}_{\varepsilon,0} \begin{pmatrix} D_{\nu_2}(iz) \\ -\frac{1}{\varepsilon} D_{\nu_2+1}(iz) \end{pmatrix}. \quad (14)$$

Here $D_\nu(z)$ is the parabolic cylinder function, $z \equiv z(x) = \sqrt{2}(x - k_y)$, $\nu_1 = \varepsilon^2$, $\nu_2 = -(\varepsilon^2 + 1)$. If the wave function is required to be square integrable on the whole interval $-\infty < z < \infty$, we must set $\varepsilon^2 = n$ (where n is a non-negative integer), and $c_2 = 0$ (because wave functions with imaginary arguments blow up). These constraints determine the Landau quantized energies $\varepsilon = \pm\sqrt{n}$ and wave functions for electrons in graphene.

A. Inclusion of a square well

In the scaled shifted variable z the square-well potential $U(x) = U_0\Theta(|x| - L)$ reads

$$u(z) = \begin{cases} 0, & z(-L) < z < z(L) \\ u_0, & \text{otherwise} \end{cases}, \quad (15)$$

where $u_0 = \frac{\ell U_0}{\hbar v_F}$ and $z(L) = \sqrt{2}L - k_y \equiv L_1$, $z(-L) = -\sqrt{2}L - k_y \equiv L_2 \neq -z(L) = -L_1$, hence $k_y = -\frac{1}{2}[z(L) + z(-L)]$. Thus, a symmetric well in x is not symmetric in z . The eigenvalue problem is specified by the set of equations defined for $-\infty < z < \infty$:

$$\left[-i\sigma_x \frac{d}{dz} - \frac{1}{2}z\sigma_y \right]\psi(z) = \begin{cases} \varepsilon\psi(z), & z \in [L_2, L_1] \\ (\varepsilon - u_0)\psi(z), & z \notin [L_2, L_1]. \end{cases} \quad (16)$$

Here $\psi(z) = \begin{pmatrix} \psi^{(1)}(z) \\ \psi^{(2)}(z) \end{pmatrix}$, and ε is the energy eigenvalue that needs to be determined. As in Eq. (14), the solutions can be expressed in terms of parabolic cylinder functions $D_\nu(\cdot)$, and the spinor wave function is required to be continuous everywhere and square integrable. For $z \in [L_2, L_1]$ the solution reads,

$$\psi_c(z) = c_1 \begin{pmatrix} D_{\nu_1}(z) \\ -i\varepsilon D_{\nu_1-1}(z) \end{pmatrix} + c_2 \bar{\delta}_{\varepsilon,0} \begin{pmatrix} D_{\nu_2}(iz) \\ -\frac{1}{\varepsilon} D_{\nu_2+1}(iz) \end{pmatrix}. \quad (17)$$

Generically, the orders $\nu_1 = \varepsilon^2$, $\nu_2 = -(\varepsilon^2 + 1)$ in Eq. (17) are not (non-negative) integers. In the external regions $z \notin [L_2, L_1]$, the only solutions of the second of Eq. (16) that decay as $|z| \rightarrow \infty$ are such that: (1) the order ν of $D_\nu(\cdot)$ should be a non-negative integer, and (2) the argument of $D_\nu(\cdot)$ must be real [24]. The most general solution is then an infinite linear combination of Landau functions $L_{sn}(z) = \begin{pmatrix} D_n(z) \\ si\sqrt{n}D_{n-1}(z) \end{pmatrix}$, $n = 0, 1, \dots$, $s = \mp$.

B. Analytic solution for a special case

A general numerical solution is worked out in subsection 2 of the Appendix. Here we show that analytic solutions exist for specific discrete values of the potential

strength u_0 . We employ the following solutions of Eq. (16) for $z \notin [L_2, L_1]$, with $\varepsilon = u_0 \pm \sqrt{n}$, that is, $n = (\varepsilon - u_0)^2$:

$$\begin{aligned} w\psi_{\text{right}}(z) &= c_3\Theta(z - L_1)\begin{pmatrix} D_n(z), \\ \pm i\sqrt{n}D_{n-1}(z) \end{pmatrix}, \\ \psi_{\text{left}}(z) &= c_4\Theta(L_2 - z)\begin{pmatrix} D_n(z) \\ \pm i\sqrt{n}D_{n-1}(z) \end{pmatrix}. \end{aligned} \quad (18)$$

1. Matching equations

Following Eqs. (17) and (18), for fixed $\pm\sqrt{n}$, the wave function is determined by the coefficients vector $\mathbf{c} = (c_1, c_2, c_3, c_4)^T$. Continuity requires $\psi_c(L_1) = \psi_{\text{right}}(L_1)$ and $\psi_c(L_2) = \psi_{\text{left}}(L_2)$, where each relation yields two equations. This set of four linear homogeneous equations can be formally written as $A_n(u_0)\mathbf{c} = 0$. The potential strength u_0 must satisfy $\text{Det}[A_n(u_0)] = 0$, and the roots u_{nm} determine the bound-state energies $\varepsilon_{nm} = u_{nm} \pm \sqrt{n}$. The eigenvector \mathbf{c}_{nm} of $A_n(u_{nm})$ corresponding to eigenvalue zero determines the wave function in all space. Figure 4(a) plots $\text{Det}[A_n(u_0)]$ versus u_0 . For each $0 \leq n \in \mathbb{Z}$ there are, in principle, an infinite number of zeros $\{u_{nm}\}$ and infinite number of bound-state energies $\varepsilon_{nms} = u_{nm} + s\sqrt{n}$, where $s = \pm$. A few bound state energies are shown in Fig. 4(b).

2. Wave functions and currents

The spinor wave functions and the currents along y corresponding to well height u_{nm} for $(n, m) = (0, 0)$ are shown in Fig. 5. The main properties of the wave functions are: (1) It is possible to choose the phase such that the upper component of the spinor is real while the lower component is imaginary. This implies that the current along x vanishes, as it should for bound states. (2) Parity symmetry (or antisymmetry) is not exact for the wave functions around $z = 0$. The density $\rho(z) = \psi_0^\dagger(z)\psi_0(z)$ is not perfectly symmetric and the current density $J_y(z) = \psi_0^\dagger(z)\sigma_y\psi_0(z)$ is not perfectly antisymmetric, hence the total (integrated) current I_y does not vanish. (With the choice of parameters adopted here we get $I_y = 0.007373$). The reason for this is that the energy levels are degenerate $\varepsilon(k_y) = \varepsilon(-k_y)$ and the corresponding quantities for $\pm k_y$ are related as:

$$\rho(z; -k_y) = \rho(-z; k_y), \quad J_y(z; -k_y) = -J_y(-z; k_y). \quad (19)$$

Hence, the (incoherent) weighted sums of contributions from $\pm k_y$ satisfy the pertinent symmetries and hence $I_y = 0$ for the weighted sums. In principle, $\rho(z)$ and $J_y(z)$ can be measured, as can the dipole transition rates. Therefore, graphene Landau wave functions with noninteger orders can be probed. In the calculations of density, current, and E_1 transitions presented below we take $u_0 = \frac{\ell U_0}{\hbar v_F} = 10$, $-\frac{5}{2\sqrt{2}} \leq x \leq \frac{5}{2\sqrt{2}}$ (in units of ℓ) and $k_y = \pm 0.5$ (in units of $1/\ell$). Since $z = \sqrt{2}x - k_y$, this gives $[L_2, L_1] = [-3, 2]$ for $k_y = +0.5$ and $[L_2, L_1] = [-2, 3]$ for $k_y = -0.5$.

Figure 6 shows the symmetrized ground-state density $\rho_0(z) = \frac{1}{2} \sum_{\pm k_y} [\psi_0^\dagger(z)\psi_0(z)]$ and current density along y , $J_{y0}(z) = \frac{1}{2} \sum_{\pm k_y} [\psi_0^\dagger(z)\sigma_y\psi_0(z)]$. As stated in Eq. (19), the incoherent sum of contributions from $\pm k_y$ results in a symmetric density and an antisymmetric current density. In particular, the total current along y , $I_{y0} = \int_{-\infty}^{\infty} J_{y0}(z)dz$, vanishes (as it

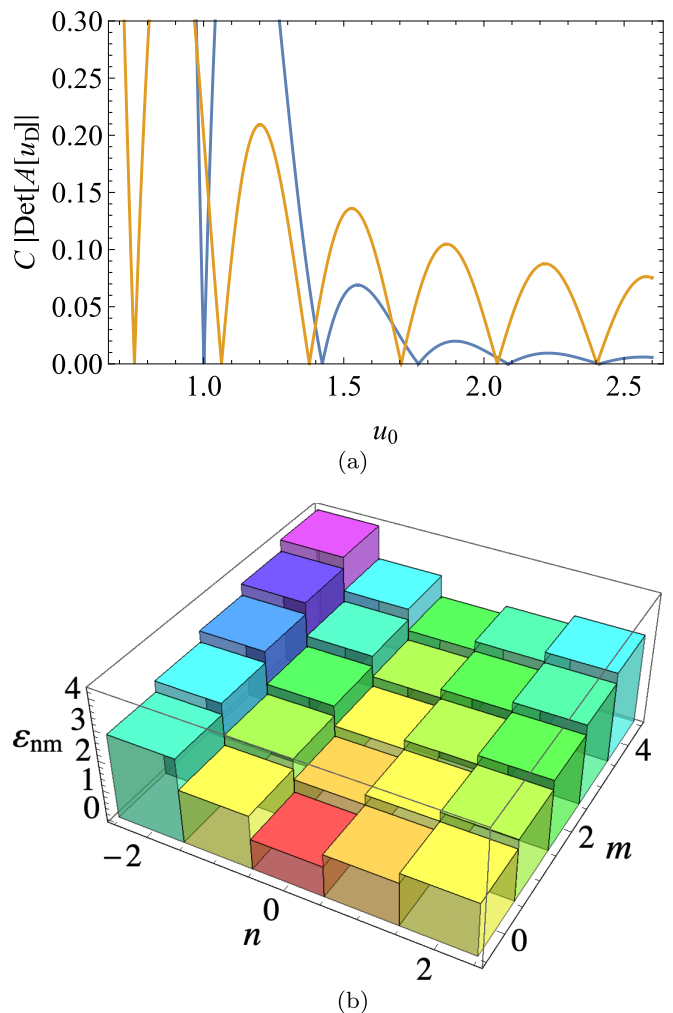


FIG. 4. (a) For square well boundary conditions with $L_2 = -3.1\sqrt{2}$ and $L_1 = 2.1\sqrt{2}$ (in units of ℓ) we plot $|\text{Det}[A_n(u_0)]|$ as a function of u_0 for $n = 0$ (blue) and $n = 1$ (orange). The zeros u_{nm} fix the bound-state energies, $\varepsilon_{nm} = u_{nm} \pm \sqrt{n}$, $n = 0, 1, 2, \dots$, $m = 0, 1, 2, \dots$ (b) 3D discrete plot of the bound-state energies ε_{nm} (negative n means $\varepsilon_{nm} = u_{nm} - \sqrt{n}$). The points (n, m, ε_{nm}) are the center of a unit square placates with half integer vertices, $(n \pm 1/2, m \pm 1/2)$. The square placates are drawn simply to graphically clarify the values of ε_{nm} .

should). Similar results for the first excited state $\psi_1(x)$ are shown in Fig. 7.

C. E_1 transitions in the presence of a magnetic field

In analogy with the discussion of photon absorption in the absence of an external magnetic field (see Sec. IV), we now consider E_1 transitions in the presence of the magnetic field. The E_1 transition rates $w_{n,m}$ from m to n with light polarized along the x axis are proportional to $|\varepsilon_n - \varepsilon_m|^4 |\langle \psi_n | x | \psi_m \rangle|^2$, where $\{\varepsilon_n\}$ are the energy eigenvalues obtained from the solution of Eq. (A11) in the Appendix, and the transition dipole matrix elements are

$$\langle x \rangle_{nm} = \langle \psi_m | x | \psi_n \rangle = \int_{-\infty}^{\infty} \psi_m^\dagger[z(x)]x\psi_n[z(x)]dx, \quad (20)$$

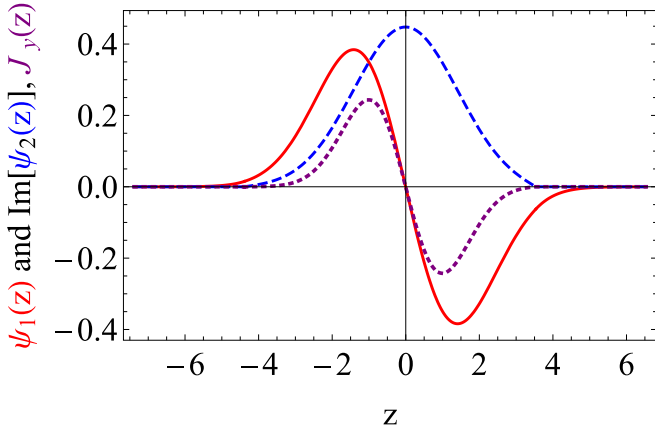


FIG. 5. For the potential strength $u_0 = u_{n=0,m=0} = 1.0013$ [the first blue zero in Fig. 4(a)] and $L_2 = -3.1\sqrt{2}$, $L_1 = 2.5\sqrt{2}$, we plot the upper component (solid red) and $-i$ times the lower component (dashed blue) of the wave function $\psi_{10}(z)$, and the current $J_y(z)$ (dotted purple) of the state $\psi_{00}(z)$. Since u_{00} is small, the wave functions and current seem to have symmetry around $z = 0$ but, in fact, they do not. To get the quantities in physical units recall that z , $\psi(z)$ and $J(z)$ are in units of ℓ , $1/\sqrt{\ell}$ and $1/\ell$, respectively.

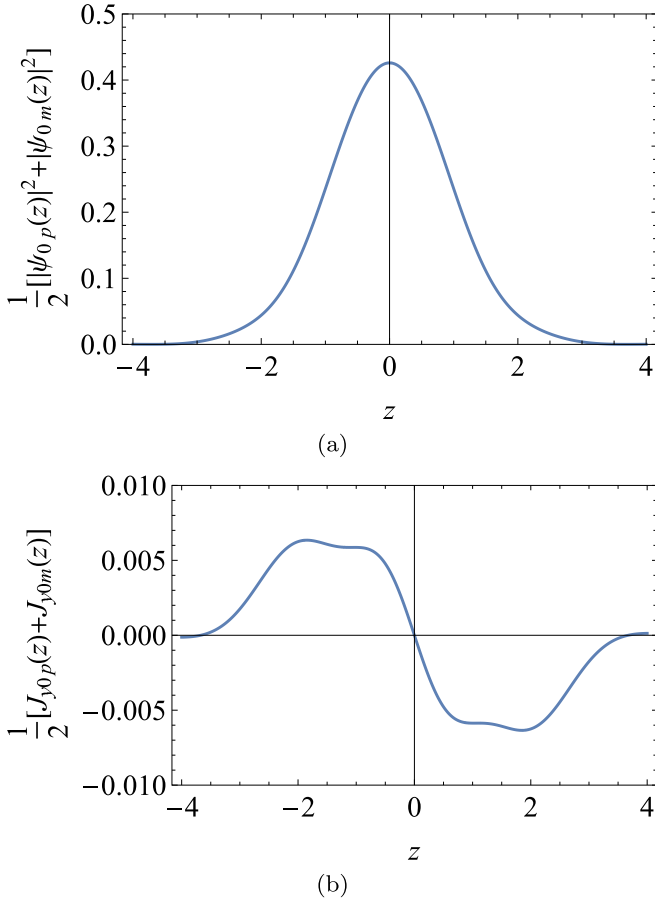


FIG. 6. Density $\rho_0(z)$ and current $J_{y0}(z)$ of the ground state $\psi_0(z)$ following incoherent summation over $\pm k_y$. (a) $\frac{1}{2}[\rho_0(z, k_y) + \rho_0(z, -k_y)]$, (b) $\frac{1}{2}[J_{y0}(z, k_y) + J_{y0}(z, -k_y)]$. $\rho(z)$ and $J(z)$ are in units of $1/\ell$.

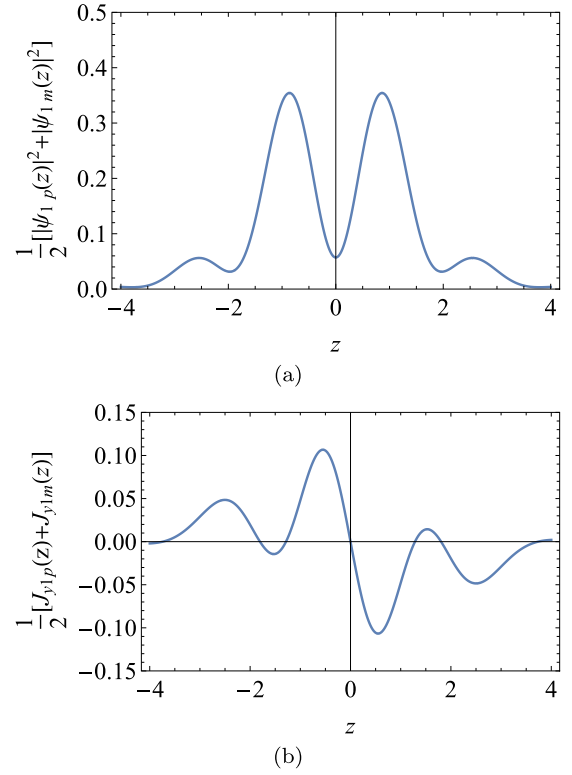


FIG. 7. Density $\rho_1(z)$ and current $J_{y1}(z)$ of the first excited state $\psi_1(z)$ following incoherent summation over $\pm k_y$. (a) $\frac{1}{2}[\rho_1(z, k_y) + \rho_1(z, -k_y)]$, (b) $\frac{1}{2}[J_{y1}(z, k_y) + J_{y1}(z, -k_y)]$. $\rho(z)$ and $J(z)$ are in units of $1/\ell$.

where $z(x) = \sqrt{2}(x - k_y)$. The main contribution comes from the interval $-L \leq x \leq L$ where $L/\ell = \frac{5}{2\sqrt{2}}$ (see caption of Fig. 5). The photon absorption spectrum between the lowest eight states $n = 0, 1, \dots, 7$ (determined by the set of parameters specified after Fig. 5), is shown in Fig. 8. It is interesting to note the differences between photon absorption spectra in the presence and in the absence of the magnetic field shown in Fig. 2. In the latter case, there is the usual parity selection rule, namely, the function $\psi_n^\dagger(x)x\psi_m(x)$ is even (odd) if $n + m + 1$ is odd (even). In particular, transitions

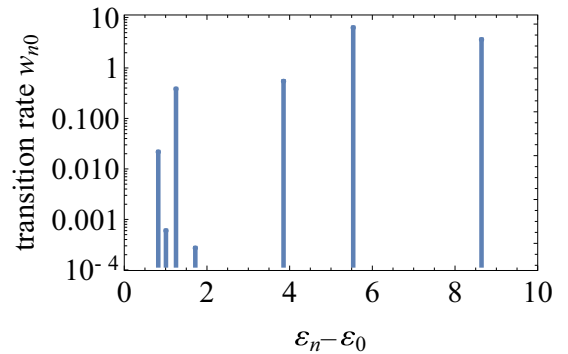


FIG. 8. Absorption spectrum of the transitions $0 \rightarrow n$, $n = 1, 2, \dots, 7$. The transition rates w_{n0} (in dimensionless units), which are proportional to $\omega_{0n}^4 |\langle \psi_0 | x | \psi_n \rangle|^2$, are plotted versus the resonant light photon energy $\hbar\omega_{0n} = \varepsilon_n - \varepsilon_0$ in dimensionless units.

$0 \rightarrow 1, 3, 5, 7$ are shown but $0 \rightarrow 2, 4, 6$ vanish. These parity selection rules do not apply in the presence of magnetic field, hence all transitions $0 \rightarrow n$ ($n = 1, 2, \dots, 7$) are allowed.

Following Ref. [21], p. 324, the electric dipole (E_1) transition rate w_{mn} between states $|n\rangle$ and $|m\rangle$ is given by

$$w_{mn} = A(E_m - E_n)^4 (e\mathcal{E}_x)^2 |X_{mn}|^2, \quad X_{mn} = \langle m|x|n\rangle,$$

where A is a constant depending on e , c , and \hbar . E_m and E_n are the pertinent energy levels and \mathcal{E}_x is the slowly varying electric field envelope. The physical dimension of the rates w_{mn} are s^{-1} . Recall that the parameter of length here is the magnetic length ℓ (in the presence of a magnetic field of 1 T, $\ell \approx 25$ nm, the energy unit is $\hbar v_F/\ell \approx 27.52$ meV), hence the measured physical quantities, expressed in terms of our dimensionless quantities, ε_m , u_0 , and x_{mn} are

$$E_m = \frac{\hbar v_F}{\ell} \varepsilon_m, \quad U_0 = \frac{\hbar v_F}{\ell} u_0, \quad X_{mn} = \ell x_{mn},$$

$$w_{mn} = A \left[\frac{\hbar v_F}{\ell} \right]^4 (\varepsilon_n - \varepsilon_m)^4 (e\mathcal{E}_x \ell)^2 |x_{mn}|^2. \quad (21)$$

VII. SUMMARY AND CONCLUSIONS

We have developed a formalism for studying electron Klein bound states in single layer graphene subject to a symmetric 1D square-well potential, in the absence as well as in the presence of an external magnetic field. This study completes and adds novel concepts to the analysis of chiral tunneling reported Ref. [2]. In the absence of magnetic field, an analytic expression is derived for the wave functions of the ground and excited states, and a beautiful symmetry between the two components of the (pseudo)spinor is shown to exist. We showed that Klein bound states are located both below the barrier ($u_0 - k_y < \varepsilon < u_0$) and above the barrier ($u_0 < \varepsilon < u_0 + k_y$). In both cases, bound states exist also within the Schrödinger scheme, but in that case the dependence of the energy interval that hosts bound states on k_y is quadratic. The consequences of parity noninvariance and time reversal invariance are elucidated, and photon absorption inducing E_1 transitions between levels are worked out. For the sake of completeness we illustrated the structure of the transmission coefficient $T(\varepsilon)$ across the entire positive energy axis.

In the presence of an external uniform perpendicular magnetic field, an analytic expression for the wave functions is derived for a discrete (albeit infinite) sequence of potential strengths $u_0 = \{u_{nm}\}$ $n, m = 0, 1, 2, \dots$. Hence, the Landau functions in graphene with noninteger orders and imaginary argument appearing in Eq. (17) can be experimentally investigated. Numerical calculations valid for arbitrary potential strength are presented in the Appendix, and the importance of the symmetry (19) is stressed.

Our results can be applied directly to the propagation of light waves in periodic waveguide optical structures. Light transport in a 2D binary photonic superlattice with two interleaved lattices A and B is realized by a sequence of equally spaced waveguides with alternating deep/shallow peak refractive index changes. The propagation of monochromatic light waves are modeled by the scalar wave equation in the

paraxial approximation, and the tight-binding limit results in coupled-mode equations for the fundamental-mode field amplitudes which are functions of a discrete set of integer variables. Approximating these with a continuous variable, rather than as an integer index, yields a 2D Dirac equation with an external electrostatic potential [15,16]. This yields the same mathematical formalism used here.

ACKNOWLEDGMENTS

We thank Mikhail I. Katsnelson, Jean Noël Fuchs, Ken Shiozaki, and Ady Stern for illuminating discussions. This work was supported in part by a grant from the DFG through the DIP program (FO703/2-1).

APPENDIX

In this short Appendix we elaborate on two points discussed in the main text. Subsection 1 explains the construction and displays the precise form of the matrix $A(\varepsilon)$ introduced in Eq. (5). Subsection 2 details the numerical solution of Eq. (16).

1. The Matrix $A(\varepsilon)$ Related to Eq. (5)

Here we give an explicit expression for the matrix $A(\varepsilon)$ introduced in Eq. (5) that determines the bound state energies and wave function coefficients specified by the vector $\mathbf{c} \equiv (a, b, \alpha, \delta)$ appearing in Eq. (2). The pertinent quantities are introduced after Eq. (5), and Eqs. (3) and (A2). For self-consistency, some equations are repeated. The (dimensionless) momenta inside the well ($u_0 = 0$) and outside the well ($u_0 > \varepsilon > 0$) are,

$$k_x = \varepsilon \cos \phi, \quad k_y = \varepsilon \sin \phi, \quad \tan \phi = \frac{k_y}{k_x},$$

$$q_x = \sqrt{(\varepsilon - u_0)^2 - k_y^2}, \quad \tan \theta = \frac{k_y}{q_x}. \quad (A1)$$

In the p - n - p junction analyzed here, the Klein paradox occurs if the inequality $u_0 > \varepsilon > 0$ is satisfied. Klein bound states occur under the more stringent inequality,

$$u_0 > \varepsilon > u_0/(1 + \sin \phi) > 0 \Rightarrow q_x$$

$$= i\kappa_x = i\sqrt{(\varepsilon \sin \phi)^2 - (u_0 - \varepsilon)^2}, \quad (A2)$$

where $\kappa_x > 0$ (real and positive). The bound-state wave functions must decay exponentially as $e^{-\kappa_x|x|}$ as $|x| \rightarrow \infty$. In this region $\tan \theta = -ik_y/\kappa_x$ is pure imaginary, and $\tan^2 \theta < -1$. To ensure this behavior we must set $\beta = \gamma = 0$ in Eq. (2), keeping only the decaying parts of the wave function for $|x| > 1$. The matching conditions at $x = \pm 1$ lead to a homogeneous system of four linear equations for the complex coefficients a, b, α, δ . Bound-state solutions occur at energies $\{\varepsilon_n\}$ for which the determinant of $A(\varepsilon)$ vanishes, and the

corresponding coefficient vector \mathbf{c}_n is determined by the set of homogeneous equations $A(\varepsilon_n)\mathbf{c}_n = 0$. The explicit form of the matrix $A(\varepsilon)$ in the system of equations, $A(\varepsilon)\mathbf{c} = 0$, is given by

$$A(\varepsilon) = \begin{pmatrix} e^{i\varepsilon \cos \phi} & e^{-i\varepsilon \cos \phi} & -e^{-\kappa_x} & 0 \\ e^{i(\varepsilon \cos \phi + \phi)} & -e^{-i(\varepsilon \cos \phi + \phi)} & e^{(-\kappa_x + i\theta)} & 0 \\ e^{-i\varepsilon \cos \phi} & e^{i\varepsilon \cos \phi} & 0 & -e^{-\kappa_x} \\ e^{-i(\varepsilon \cos \phi - \phi)} & -e^{i(\varepsilon \cos \phi - \phi)} & 0 & -e^{(-\kappa_x - i\theta)} \end{pmatrix}. \quad (\text{A3})$$

The determinant is given by

$$\text{Det}[A] = 4e^{-2\kappa_x} [\cos \theta \cos \phi \cos(2\varepsilon \cos \phi) + i(1 + \sin \theta \sin \phi) \sin(2\varepsilon \cos \phi)]. \quad (\text{A4})$$

Here $\tan \theta = \frac{\varepsilon \sin \phi}{q_x}$ and for $\frac{u_0}{1 + |\sin \phi|} < \varepsilon < u_0$ we have $q_x^2 = (u_0 - \varepsilon)^2 - (\varepsilon \sin \phi)^2 = -\kappa_x^2 < 0$. In this case $\sin \theta$ is real and $\cos \theta$ is imaginary, so that, up to a multiplicative constant, the determinant is real in this energy range. After some algebra one arrives at the expression in Eq. (5). In the interval $u_0 < \varepsilon < \frac{u_0}{1 - |\sin \phi|}$, where we find bound states as in Fig. 3(a), the appropriate matrix $\tilde{A}(\varepsilon)$ is obtained after reversing the signs of $A(2, 3)$ and $A(4, 4)$. The corresponding determinant is:

$$\text{Det}[\tilde{A}] = 4e^{-2\kappa_x} [\cos \theta \cos \phi \cos(2\varepsilon \cos \phi) + i(1 - \sin \theta \sin \phi) \sin(2\varepsilon \cos \phi)]. \quad (\text{A5})$$

2. Numerical solution of Eq. (16)

The set of Landau functions is complete on the interval $(-\infty, \infty)$ so we can expand $\psi(z)$:

$$\psi(z) = \sum_{n=0}^{M \rightarrow \infty} \sum_{s=\mp} a_{ns} L_{ns}(z),$$

where $L_{ns}(z) = N_{ns} \begin{pmatrix} D_n(z), \\ si\sqrt{n}D_{n-1}(z) \end{pmatrix}$. (A6)

Here N_{ns} is a normalization factor. Substitution into Eq. (16) then yields

$$[-i\sigma_x \partial_z - \frac{1}{2}z\sigma_y]\psi(z) = \sum_{n=0}^M \sum_{s=\mp} a_{ns} s\sqrt{n} L_{ns}(z) = [\varepsilon - u(z)] \sum_{n=0}^M \sum_{s=\mp} a_{ns} L_{ns}(z). \quad (\text{A7})$$

Multiplying by $L_{mt}^\dagger(z)$ (where $t = \mp$) and integrating over z , using $\langle L_{mt} | L_{ns} \rangle = \delta_{mt} \delta_{ts}$ one obtains

$$t\sqrt{m}a_{mt} = \varepsilon a_{mt} - \sum_{n=0}^M \sum_{s=\pm} A_{mt,ns} a_{ns}. \quad (\text{A8})$$

The infinite sum (as $M \rightarrow \infty$) can be cut off at a sufficiently large M . This procedure leads to an eigenvalue problem in a finite Hilbert space of dimension $2M + 1$. The matrix A introduced above can be written as $u_0(I - B)$, where I is the $(2M + 1) \times (2M + 1)$ unit matrix. The explicit expressions for the matrices A and B are

$$A_{mt,ns} = \int_{-\infty}^{\infty} L_{mt}^\dagger(z) u(z) L_{ns}(z) dz = u_0 \underbrace{[\delta_{mt} \delta_{ts}]}_{I_{mt,ns}} - \underbrace{\int_{L_2}^{L_1} L_{mt}^\dagger(z) L_{ns}(z) dz}_{B_{mt,ns}}. \quad (\text{A9})$$

where u_0 is the strength of the square well potential defined in Eq. (17). Next, we define a diagonal matrix Λ by

$$\Lambda_{mt,ns} = \delta_{mt,ns} \text{Diag}(t\sqrt{m}) = (0, \sqrt{1}, \sqrt{2}, \dots, \sqrt{M}, -\sqrt{1}, -\sqrt{2}, \dots, -\sqrt{M}), \quad (\text{A10})$$

and a vector \mathbf{a} with $2M + 1$ components, $a_{ns} = (a_{0+}, a_{1+}, a_{2+}, \dots, a_{M+}, a_{1-}, a_{2-}, \dots, a_{M-})$. Equation (A8) then becomes the eigenvalue problem,

$$[\Lambda + u_0(I - B)]\mathbf{a} = \varepsilon \mathbf{a}. \quad (\text{A11})$$

The matrix $\Lambda + u_0(I - B)$ is real and symmetric. For $u_0 = 0$ the eigenvalues are the Landau energies for graphene $\varepsilon_m = \pm\sqrt{m}$.

- [1] O. Klein, *Z. Phys.* **53**, 157 (1929); https://en.wikipedia.org/wiki/Klein_paradox.
 [2] M. I. Katsnelson, K. S. Novoselov, and A. K. Geim, *Nat. Phys.* **2**, 620 (2006).
 [3] B. Huard, J. A. Sulpizio, N. Stander, K. Todd, B. Yang, and D. G. Gordon, *Phys. Rev. Lett.* **98**, 236803 (2007).
 [4] A. F. Young and P. Kim, *Nat. Phys.* **5**, 222 (2009).
 [5] O. Roslyak, A. Iurov, G. Gumbs, and D. Huang, *J. Phys.: Condens. Matter* **22**, 165301 (2010).
 [6] Pierre E. Allain and J. Fuchs, *Eur. Phys. J. B* **83**, 301 (2011).
 [7] L. Brey and H. A. Fertig, *Phys. Rev. B* **73**, 235411 (2006); D. S. Novikov, *ibid.* **76**, 233402 (2007); Kumar S. Gupta and S. Sen, *Mod. Phys. Lett.* **24**, 99 (2009); N. M. R. Peres,

- J. Phys.: Condens. Matter* **21**, 095501 (2009); J. W. González, M. Pacheco, L. Rosales, and P. A. Orellana, *Europhys. Lett.* **91**, 66001 (2010); P. M. Krstajić and P. Vasilopoulos, *J. Phys.: Condens. Matter* **23**, 135302 (2011); C. A. Downing, D. A. Stone, and M. E. Portnoi, *Phys. Rev. B* **84**, 155437 (2011); D. A. Stone, C. A. Downing, and M. E. Portnoi, *ibid.* **86**, 075464 (2012); J. W. González, M. Pacheco, L. Rosales, and P. A. Orellana, *ibid.* **83**, 155450 (2011); P. Ghosh and P. Roy, *Phys. Lett. A* **380**, 567 (2016).
 [8] J. M. Pereira Jr., V. Mlinar, F. M. Peeters, and P. Vasilopoulos, *Phys. Rev. B* **74**, 045424 (2006).
 [9] M. Barbier, P. Vasilopoulos, and F. M. Peeters, *Philos. Trans. R. Soc. London A* **368**, 5499 (2010).

- [10] M. R. Masir, P. Vasilopoulos, and F. M. Peeters, *New J. Phys.* **11**, 095009 (2009).
- [11] M. R. Masir, P. Vasilopoulos and F. M. Peeters, *Phys. Rev. B* **79**, 035409 (2009).
- [12] H. C. Nguyen, M. T. Hoang, and V. L. Nguyen, *Phys. Rev. B* **79**, 035411 (2009).
- [13] R. R. Hartmann, N. J. Robinson, and M. E. Portnoi, *Phys. Rev. B* **81**, 245431 (2010); R. R. Hartmann and M. E. Portnoi, *Phys. Rev. A* **89**, 012101 (2014); C. A. Downing and M. E. Portnoi, *Phys. Status Solidi B* **256**, 1800584 (2019).
- [14] C. Gutiérrez, L. Brown, C.-J. Kim, J. Park, and A. N. Pasupathy, *Nat. Phys.* **12**, 1069 (2016).
- [15] S. Longhi, *Phys. Rev. B* **81**, 075102 (2010).
- [16] S. Longhi, *Appl. Phys. B* **104**, 453 (2011).
- [17] A. H. Castro Neto, F. Guinea, N. M. R. Peres, K. S. Novoselov, and A. K. Geim, *Rev. Mod. Phys.* **81**, 109 (2009).
- [18] Riazuddin, [arXiv:1105.5956](https://arxiv.org/abs/1105.5956).
- [19] E. Sadurni, E. Rivera-Mocinos, and A. Rosado, *Rev. Mex. Fis.* **61**, 170 (2015).
- [20] The reason is that there are two inequivalent representations of the 2D Dirac γ matrices. Parity operation carries valley $\mathbf{K} \rightarrow \mathbf{K}'$, and its conservation can be restored if valley degeneracy is incorporated in the Lagrangian, when it is built upon both representations [18].
- [21] Y. B. Band and Y. Avishai, *Quantum Mechanics, with Applications to Nanotechnology and Quantum Information Science* (Academic Press–Elsevier, Oxford, UK, 2013), Sec. 7.9.4.
- [22] V. Barone, O. Hod, and G. E. Scuseria, *Nano Lett.* **6**, 2748 (2006).
- [23] Z. Lenarcic, *Landau Levels in Graphene*, http://www-fl.ijs.si/~ramsak/Nanofizika/grafen/zala_lenarcic_grafen.pdf.
- [24] F. W. J. Olver, Uniform asymptotic expansions for weber parabolic cylinder functions of large orders, *Journal of Research of the National Bureau of Standards B. Mathematics and Mathematical Physics* **63B**, 131 (1959).